3D Efflux Velocity Characteristics of Marine Propeller Jets

Hamill, G. A., Kee, C., & Ryan, D. (2015). 3D Efflux Velocity Characteristics of Marine Propeller Jets. *Proceedings of the ICE - Maritime Engineering*, *168*(2), 62-75. https://doi.org/10.1680/jmaen.14.00019

Maritime Engineering
Volume 168 Issue MA2
Three-dimension efflux velocity characteristics of marine propeller jets
Hamill, Kee and Ryan

ice | proceedings

Proceedings of the Institution of Civil Engineers
Maritime Engineering 168 June 2015 Issue MA2
Pages 62–75 http://dx.doi.org/10.1680/maen.14.00019
Paper 2014-19
Received 16/10/2014 Accepted 16/04/2015
Keywords: coastal engineering/hydraulics & hydrodynamics/ports, docks & harbours

ice Institution of Civil Engineers
publishing

Three-dimension efflux velocity characteristics of marine propeller jets

Gerard Hamill BSc, PhD
School of Planning, Architecture and Civil Engineering, Queen's University Belfast, Northern Ireland

Charmaine Kee BEng, PhD
Hydro NI, Omagh Enterprise Centre, Omagh, Northern Ireland

Dona Ryan BEng, PhD, CEng, MICE, MIEI
Bellaghy, Co. Derry. Northern Ireland

Determining the efflux velocity in a ship's propeller jet is the key to calculating the velocity at any other location within the diffusing jet. Current semi-empirical equations used to calculate the magnitude of the efflux velocity have been based on studies that employed a limited range of propeller characteristics. This paper reports on the findings of an experimental investigation into the magnitude of the efflux velocities of the jets produced by four different propellers, where the characteristic of the blade geometry has been chosen to extend the range of applicability of the outcomes. Measurements of velocity have been made using a three-dimensional laser Doppler anemometry system, with the test propellers operating at a range of rotational speeds that bound typical operational values. Comparisons are made with current predictive theories and, to aid engineers in the design of marine infrastructure, methods are presented by which the three-dimensional efflux velocity components, as well as the resultant efflux value, can be more accurately determined.

Notation

C_t	thrust coefficient of propeller
D_h	diameter of hub (m)
D_p	diameter of propeller (m)
E_0	gradient coefficient as defined in Equation 4
L_m	characteristic length (m)
N	number of propeller blades
n	propeller speed of rotation (r/min)
P'	propeller pitch to diameter ratio
R_0	resultant velocity (m/s)
R^2	coefficient of determination
$R_{e\ flow}$	Reynolds number of jet flow
$R_{e\ prop}$	Reynolds number of propeller
R_h	radius of propeller hub (m)
R_{m0}	radial distance from propeller axis to location of efflux velocity (m)
R_p	radius of propeller (m)
U_0	maximum rotational velocity along efflux plane (m/s)
V_0	maximum axial velocity along efflux plane (m/s)
W_0	maximum radial velocity along efflux plane (m/s)
X	Cartesian co-ordinate measured laterally from face of propeller (m)
Y	Cartesian co-ordinate measured horizontally to left or right of propeller centreline (m)
Z	Cartesian co-ordinate measured vertically up or down along propeller centreline (m)
ε	gradient coefficient defined in Equation 3
ν	kinematic viscosity of fluid (m^2/s)

1. Introduction

A propeller is the most common form of marine propulsion device for ships and ferries. The impact of the turbulent high-velocity jets that are produced, by such devices, on the bed and banks of harbour basins and navigation channels can lead to serious erosion, structural undermining and costly remedial repairs. The continued mooring and unmooring of vessels at the same location can result in accumulative scour and siltation problems, as outlined by Sumer and Fredsoe (2002) and reported by Qurrain (1994). Froehlich and Shea (2000) have shown that essential cover to buried pipelines, tunnels and contained aquatic disposal sites can also be removed by propeller-induced flows. For these reasons, the effects of propeller-induced flow have received continuing worldwide attention.

The flow field produced by the action of rotating propeller blades is complex in nature. Near to the propeller, the passing blades and rotating hub influence the characteristics of the flow. The magnitude and distribution of the velocities within the dissipating jet are formulated at this initial 'efflux' plane and it is the magnitude of the maximum velocity along this plane, the 'efflux velocity', that is used by engineers in the calculation of all subsequent velocity values within the diffusing jet.

The prediction of the efflux velocity has been reported by a number of authors such as Fuehrer and Römisch (1977), Berger *et al.* (1981), Verhey *et al.* (1987) and Hamill (1987), who have based their work on the concept of axial momentum theory to describe diffusion characteristics. Hamill *et al.* (2004) found the core assumptions of this theory inadequately described the process involved. More recently Lam *et al.* (2012a) described semi-empirical methods for predicting the efflux velocity of the main axial component of the flow, based on a range of experiments with one test propeller, while Lam *et al.* (2012b) extended the discussion by including measurements of turbulence intensity.

2. Time-averaged velocity characteristics of unconfined propeller jets

The jet produced by a rotating propeller is a complex three-dimensional (3D) flow with axial, radial and rotational velocity components (Hamill *et al.*, 2003). The axial velocity is the most significant component found along the propeller axis of rotation. It is this component that is used to impart a forward thrust to the ship. The axial thrust produced by a rotating propeller will depend on the propeller geometry excluding the hub, which does not provide any forward thrust (Hamill and Johnston, 1993). As the propeller jet diffuses, a second 'rotational' velocity component is developed due to the rotation of the blades. The propeller jet can be considered to act like any other submerged jet; as it moves through the receiving waters there is an exchange of energy with the surrounding fluid. As the surrounding fluid becomes entrained into the jet there is a loss in energy with the jet expanding in size; a third 'radial' component is developed due to the radial increase in the propeller jet (Hamill *et al.*, 2003). Figure 1 shows a schematic representation of the three components that make up the flow. On the vertical plane, 'Z', just behind the propeller, a vertical component of velocity can be seen to lie along the radius of the propeller, while on the horizontal plane, 'Y', the same vertical component is tangential to the line of rotation at that point. The axial component is always located along the line of the propeller shaft. The combination of axial, radial and rotational velocity components make up the 3D flow, and the resultant velocity is found from the standard resolution of vectors in 3D space.

2.1 Axial efflux velocity, V_0

The maximum velocity taken from a time-averaged velocity distribution along the initial propeller plane is termed the efflux velocity, V_0, and it has been investigated by many researchers: Berger *et al.* (1981); Bergh and Cederwall (1981); Fuehrer and Römisch (1977); Hashmi (1993); Verhey (1983), Hamill (1987); Stewart (1992). Each have presented differing relationships that can be used to calculate the magnitude of the velocity, and the main equations that have been employed by the engineering community are summarised as follows.

Fuehrer and Römisch (1977)

$$1. \quad V_0 = 1{\cdot}59 n D_p \sqrt{C_t}$$

Hamill (1987)

$$2. \quad V_0 = 1{\cdot}33 n D_p \sqrt{C_t}$$

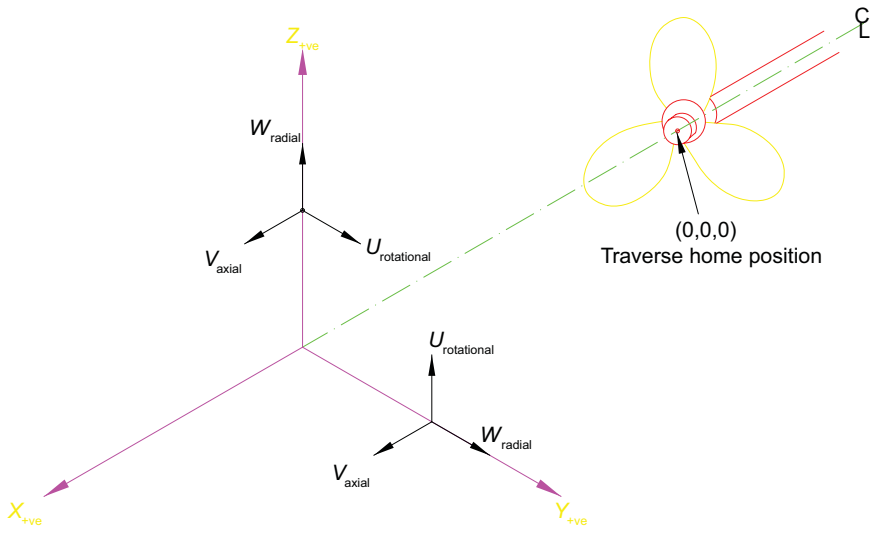

Figure 1. Schematic of velocity component directions

Stewart (1992)

$$3. \quad V_0 = \varepsilon n D_p \sqrt{C_t}$$

where

$$\varepsilon = D_p^{-0{\cdot}0686} P^{1{\cdot}519} \mathrm{BAR} - 0{\cdot}323$$

Hashmi (1993)

$$4. \quad V_0 = E_0 n D_p \sqrt{C_t}$$

where

$$E_0 = \left(\frac{D_P}{D_h}\right)^{-0{\cdot}403} (C_t)^{-1{\cdot}79} (\mathrm{BAR})^{0{\cdot}744}$$

The distance to the maximum axial velocity (symbolised by R_{m0}) is the portion of the blade where maximum thrust occurs. Berger *et al.* (1981) proposed the maximum axial velocity on the propeller efflux plane occurred at a position R_{m0} given by

$$5. \quad R_{m0} = 0{\cdot}67 R_p - R_h$$

where R_p and R_h are the radius of the propeller and hub, respectively.

McGarvey (1996) found the output solutions of Equation 5 differed from the results of an empirical investigation by up to 30%. Prosser (1986) suggested the maximum velocity in the jet occurred at approximately 60% of the blade radius from the propeller centreline, due to the low blade velocities at the hub, which produce less thrust. Work by Hamill *et al.* (2004) found the axial velocity distribution to increase from the propeller hub to a distance of approximately $0{\cdot}7R_p$ along the blade before decreasing towards the blade tips.

2.2 Rotational efflux velocity, U_0

The rotating effect of a ship's propeller causes the water to move spirally in the direction of flow about the axis of rotation, thereby containing a significant 'swirl' velocity component (Brewster, 1997). The direction of the rotationally induced flow is in the direction of rotation of the propeller blades.

The axial component of velocity was found to be the largest contributor to the resultant velocity field in the propeller wash followed in turn by the rotational and radial components (Brewster, 1997). Prosser (1986) found the magnitude of the rotational velocity was approximately 30% of the maximum axial velocity along the initial efflux plane.

To date, limited experimental investigations have been carried out examining the characteristics of the swirl, or rotational, component. Petersson *et al.* (1996) investigated the swirling jet produced by an impeller and measured the rotational component of velocity up to 12 impeller diameters from the rotating blades. It was suggested that the rotational component of velocity influenced the diffusion of the jet in the axial direction and similar effects can be observed in the wash produced by a marine propeller. Brewster (1997) analysed the characteristics of the rotational component based on a computational fluid dynamics (CFD) simulation.

Both Petersson *et al.* (1996) and Brewster (1997) observed similar trends in the rotational velocity distributions along the efflux plane. The rotational velocity profile showed two peak velocity values. One peak corresponded to the point at which the hub and the propeller blades were joined and the other was located at a point near to the tip of the propeller. Petersson *et al.* (1996) measured the first peak at $0{\cdot}15r/R_p$ and the second peak at $0{\cdot}65r/R_p$ from the propeller centreline. Brewster (1997) found these two peak velocities to occur at $0{\cdot}3r/R_p$ and $0{\cdot}8r/R_p$.

2.3 Radial efflux velocity, W_0

McGarvey (1996) carried out an experimental investigation to measure the magnitude of the radial velocity within the jets produced by two differing propellers. Previous researchers assumed the radial component of velocity was negligible within the wash of a marine propeller. However, McGarvey (1996) found the magnitude of this component was approximately 30% of the axial velocity along the face of the propeller and concluded that it should not be neglected. Brewster (1997) extracted radial velocity measurements from CFD results in order to investigate the characteristics of this component.

3. Experimental set-up

A non-intrusive optical measurement system was used to acquire the axial, radial and rotational velocity components produced by a range of test propellers operating under bollard-pull conditions. Each propeller was investigated at four differing speeds of rotation set to values that bounded typical operational values. All experiments were carried out in a free-surface tank, large enough to allow the unhindered expansion of the propeller jets investigated.

3.1 Selection of propellers

British Maritime Technology (BMT) SeaTech Limited provided on loan two four-bladed experimental propellers for this research: 92 mm and 103 mm in diameter. Two further propellers of 76 mm and 131 mm in diameter were also tested.

		Prop 1	Prop 2	Prop 3	Prop 4
Propeller diameter	D_p: mm	76	92	103	131
Hub diameter	D_h: mm	14·92	20·32	20·5	27·2
Thrust coefficient	C_t	0·402	0·2908	0·388	0·558
Pitch to diameter ratio	P'	1·0	0·735	0·8283	1·136
Blade area ratio	BAR	0·47	0·4525	0·6417	0·922
Rake angle	°	0	10	0	0
Number of blades	N	3	4	4	6

Table 1. Propeller geometric characteristics

Each of the propellers investigated varied in size as well as having differing numbers of blades (N), pitch to diameter ratios (P'), thrust coefficients (C_t), rake and blade area ratios (BARs) (Table 1). The number of propeller blades varies from three to six. The pitch to diameter ratio ranges from a minimum of 0·735 up to a maximum of 1·0. The thrust coefficient, at zero advance speeds, ranges from 0·2908 up to 0·558. The BARs vary from of 0·4525 to 0·922. The blades of the 76 mm, 103 mm and 131 mm dia. propellers have no forward inclination; that is, all blades are at 90° angles to the hub while the blades of the 92 mm dia. propeller are inclined by a further 10°. In selecting these propellers it was intended to test over a large practical variation of characteristics typical of sea-going vessels, and provide a thorough test for the current predictive theories.

Froudian scaling was used to determine the speeds of rotation tested. It has been established by Blaauw and van de Kaa (1978) that scale effects due to viscosity can be ignored if the Reynolds number for the propeller exceeds 7×10^4 and the Reynolds number for the propeller flow is greater than 3×10^3. The Reynolds number for the jet flow is given by

$$6. \quad \mathrm{R_{e\ flow}} = \frac{V_0 D_p}{v}$$

The Reynolds number for the propeller is given by

$$7. \quad \mathrm{R_{eprop}} = \frac{n D_p L_m}{v}$$

The characteristic length, L_m, depends on the BAR, propeller and hub diameters as well as the number of blades. Blaauw and van de Kaa (1978) defined this length term as follows

$$8. \quad L_m = (\mathrm{BAR}) D_p \pi \left(2N\left(1 - \frac{D_h}{D_p}\right)\right)^{-1}$$

The rotational speeds used in the programme of work were based on standard Froudian scale calculations for a generic propeller of 2·5 m in diameter, rotating at 200 r/min, and having a thrust coefficient of 0·35. This provided target speeds for the experimental propellers (1–4) of 990, 1056, 865 and 640 r/min, respectively. The propellers were operated across a range of speeds that bounded these target values, and these are listed in full in Table 2.

The Reynolds numbers for the propellers operating at these rotational speeds ranged from $1{\cdot}4 \times 10^4$ to $7{\cdot}7 \times 10^4$, while the Reynolds numbers for the propeller jet ranged from $5{\cdot}3 \times 10^4$ to 30×10^4 (Table 2). The Reynolds numbers for the propellers were, in some cases, slightly less than 7×10^4; however, Blaauw and van de Kaa (1978) and Verhey (1983) proposed these scale

Propeller diameter: mm	Propeller speed of rotation: r/min	$\mathrm{R_{e\ flow}}$	$\mathrm{R_{e\ prop}}$
76	750	$6{\cdot}4 \times 10^4$	$1{\cdot}9 \times 10^4$
	1000	$8{\cdot}6 \times 10^4$	$2{\cdot}6 \times 10^4$
	1250	$10{\cdot}7 \times 10^4$	$3{\cdot}2 \times 10^4$
	1500	$12{\cdot}8 \times 10^4$	$3{\cdot}9 \times 10^4$
92	500	$5{\cdot}3 \times 10^4$	$1{\cdot}4 \times 10^4$
	750	$7{\cdot}9 \times 10^4$	$1{\cdot}7 \times 10^4$
	1000	$10{\cdot}7 \times 10^4$	$2{\cdot}3 \times 10^4$
	1250	$13{\cdot}3 \times 10^4$	$3{\cdot}5 \times 10^4$
103	500	$5{\cdot}7 \times 10^4$	$2{\cdot}4 \times 10^4$
	750	$8{\cdot}5 \times 10^4$	$3{\cdot}7 \times 10^4$
	1000	$11{\cdot}4 \times 10^4$	$4{\cdot}9 \times 10^4$
	1250	$14{\cdot}2 \times 10^4$	$6{\cdot}1 \times 10^4$
131	350	$10{\cdot}5 \times 10^4$	$2{\cdot}7 \times 10^4$
	500	$14{\cdot}9 \times 10^4$	$3{\cdot}8 \times 10^4$
	750	$22{\cdot}5 \times 10^4$	$5{\cdot}7 \times 10^4$
	1000	$29{\cdot}9 \times 10^4$	$7{\cdot}7 \times 10^4$

Table 2. Propeller speeds of rotation and corresponding Reynolds numbers investigated

effects would be insignificant. The Reynolds numbers for the jets were all greater than 3×10^3 for the speeds of rotation investigated satisfying the criteria for Froudian scaling.

3.2 Data acquisition system

Laser Doppler anemometry (LDA) is a well-established non-intrusive technique by Yeh and Cummins (1964) for the measurement of fluid flow. The 3D LDA adopted in this research was a Dantec Dynamics three-component backscatter system with a water-cooled Stabilite 2017 5W Argon-Ion laser manufactured by Spectra Physics as the illuminating light source. Frequency shifting of 40 MHz using a Bragg cell was used to remove directional ambiguity in the velocity measurements.

The optical probe was mounted on an automatic Dantec Dynamics 3D-traverse with measurement accuracies within ± 0·05 mm in three orthogonal directions. The measurement volume was located at a distance of 240 mm from the LDA probe. Three-dimensional LDA configurations required the transformation of measurements made in a non-orthogonal coordinate system into a Cartesian system. The transformation of measurements was carried out each time the laser was setup.

The LDA technique indirectly measures the velocity of the flow by measuring the speed of the (seeding) particles suspended in the flow. The seeding material used in this study was non-spherically shaped polyamide particles having a mean particle size of 20 μm and density of 1·03 g/cm^3.

All measurements were made in fully coincident mode; that is, all three processors had to recognise a valid data point before accepting the data. The maximum data rates were determined by the rates obtained with the lowest power channel. Data rates ranged between a minimum of 30 and a maximum of 1000 particles per second.

An experimental grid was established at which velocity readings across the face of the efflux plane could be taken. The centre of the propeller hub, at the cutting edge of the propeller blades, was taken as the zero location and measurements were taken on a Y (horizontal), Z (vertical) grid in 2–5 mm steps.

4. Efflux velocity measurements

All velocity components within the propellers jets were recorded simultaneously using the LDA equipment. Analysis of the 3D flow field as well as each of the components parts was then undertaken.

4.1 Axial efflux velocity

Figures 2–5 show the distribution of the axial component of velocity across the efflux plane for all tests undertaken. The shape of these profiles follows the expected trends and the efflux velocity, V_0, is taken as the average of the two peak velocities found on either side of the jet centreline, for each respective speed of rotation. The magnitudes of the efflux velocity produced during these tests can be seen in Table 3.

Comparisons of the measured empirical results were made with the output solutions of Equations 1–4 when used to predict the magnitude of the maximum axial velocity along the efflux plane (Figures 6–9). Equation 1, derived from the actuator disc theory, was found to predict the efflux velocity within 10% of the measured values. Equation 2 suggested by Hamill (1987), having a lower efflux coefficient of 1·33, was found to

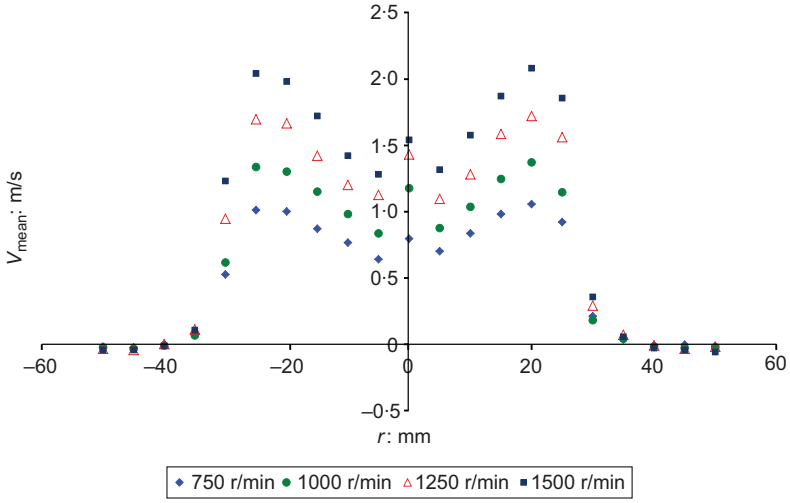

Figure 2. Axial velocity distributions on efflux plane: propeller 1

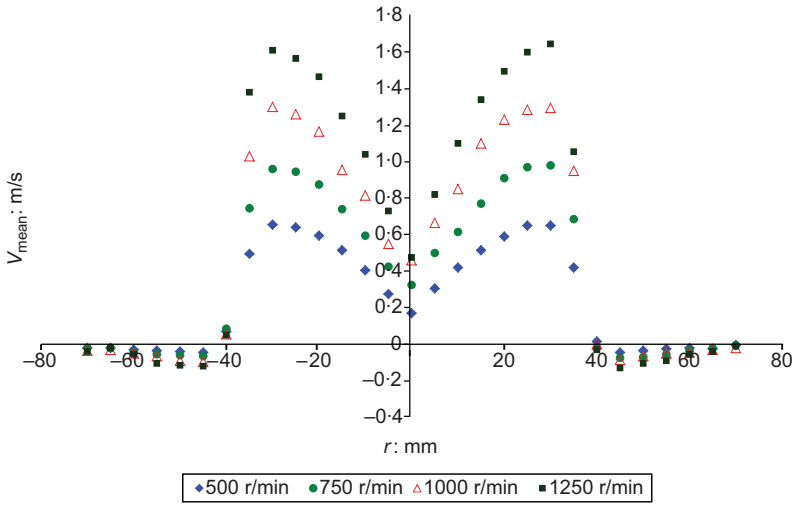

Figure 3. Axial velocity distributions on efflux plane: propeller 2

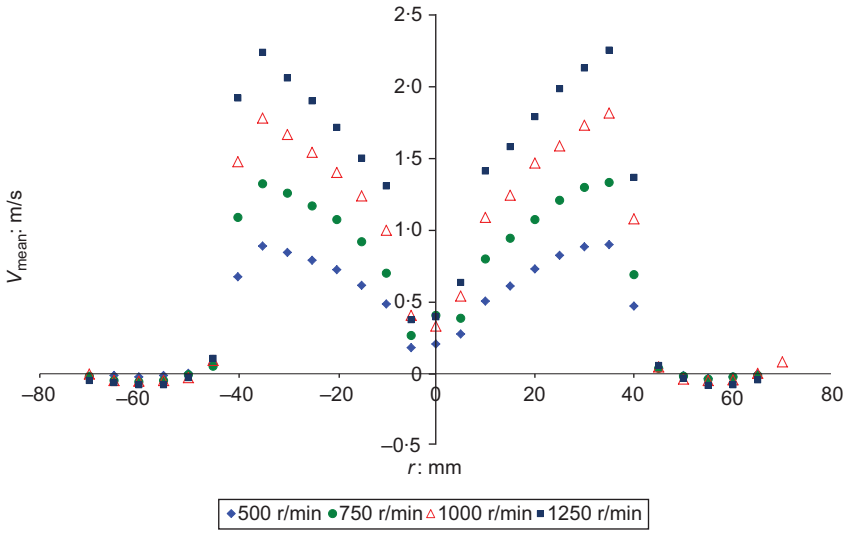

Figure 4. Axial velocity distributions on efflux plane: propeller 3

underestimate the measured efflux velocities by up to 20%. Equations 3 and 4 proposed by Stewart (1992) and Hashmi (1993), respectively, were found to underestimate the experimental efflux velocities by up to 40%. It is clear that the derivation of such semi-empirical equations from narrow test ranges, results in high errors when used to extrapolate beyond the range from which they have been derived.

A stepwise multivariate analysis of the main variables within the investigation showed that the main characteristics of influence to the axial efflux velocity were the speed of rotation (n), propeller diameter (D_p), thrust coefficient (C_t), the same variables used by all previous authors adopting the momentum theory approach. Both linear and non-linear regression algorithms were used to establish a relationship with V_0 and Equation 9 was developed, giving a coefficient of determination of $R^2 = 0{\cdot}997$.

$$9. \quad V_0 = 1{\cdot}22 n^{1{\cdot}01} D_p^{0{\cdot}84} C_t^{0{\cdot}62}$$

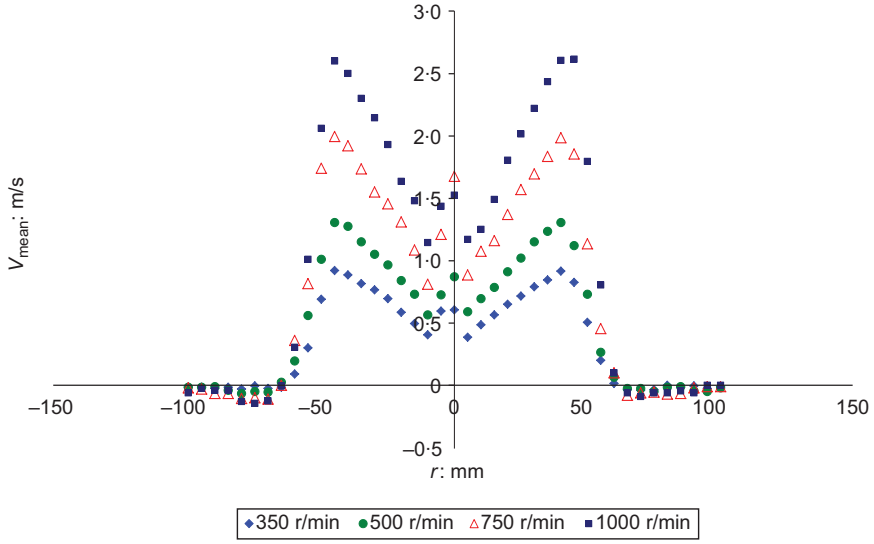

Figure 5. Axial velocity distributions on efflux plane: propeller 4

r/min	Axial: m/s	Rotational: m/s	Radial: m/s	Resultant: m/s	
Propeller 1	750	1·033	0·780	0·230	1·124
	1000	1·353	1·115	0·287	1·606
	1250	1·708	1·265	0·343	1·87
	1500	2·060	1·460	0·400	2·205
Propeller 2	500	0·653	0·400	0·140	0·702
	750	0·970	0·550	0·245	1·045
	1000	1·298	0·770	0·300	1·391
	1250	1·628	1·055	0·365	1·765
Propeller 3	500	0·890	0·710	0·165	0·931
	750	1·325	0·960	0·235	1·391
	1000	1·798	1·385	0·310	1·848
	1250	2·248	1·655	0·435	2·305
Propeller 4	350	0·918	0·63	0·155	0·977
	500	1·305	1·31	0·26	1·5
	750	1·990	1·765	0·375	2·169
	1000	2·603	2·26	0·465	2·897

Table 3. Measured values of axial, rotational, radial and resultant efflux velocities

It is proposed that in all future investigations, where the propeller characteristics lie within the ranges tested in this study, the efflux velocity is calculated using Equation 9.

Table 4 shows the corresponding measured radial locations of the efflux velocity compared to those predicted from current theory (Equation 5). The experimental ratio of R_{m0}/R_p for each of the test propellers was found to be 0·592, 0·652, 0·6796 and 0·6489. Therefore the location of R_{m0} ranged between $0{\cdot}59R_p$ and $0{\cdot}68R_p$ across the propeller radius. Percentage differences of 20%, 31%, 31% and 29% were found between the empirical results and the output solutions of Equation 5. These percentage differences, of up to 31%, indicate that Equation 5 is inaccurate in determining R_{m0}. On average the maximum velocity was found to occur at approximately 65% of the blade radius from the centre of the propeller. No consistent comparisons were found between the location of the maximum axial velocity and the location of the maximum blade area, blade thickness or chord lengths along equivalent propeller radii.

4.2 Rotational efflux velocity

The rotational velocity distribution taken along the initial efflux plane showed two peak velocity values. One peak corresponded to the point at which the hub and the propeller blades were joined and the other was present at a point near to the tip of the propeller. This distribution was evident for all experimental propellers tested and agrees with the findings of Brewster (1997) and Petersson *et al.* (1996). Figures 10 shows a plot of the distribution of measured velocity for test propeller 4, and is typical of that found for all propellers in this investigation.

In comparison to the axial efflux velocity, the rotational efflux was between 0% and 43% of the axial value and on average it was 25% lower (Table 3). This is a significant difference from the magnitudes found by Prosser (1986) who claimed the values were on average 70% lower. Investigations into the magnitudes of the consistently smaller second peak showed a

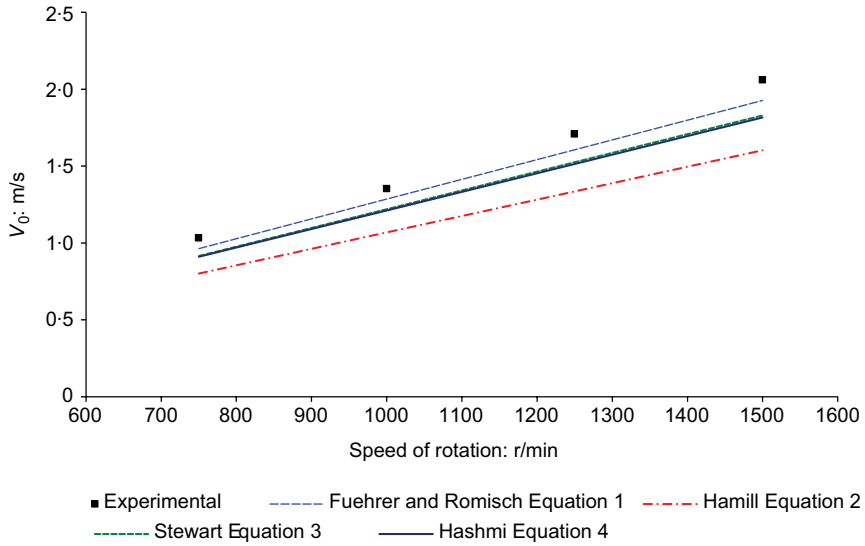

Figure 6. Comparison between measured and predicted axial efflux velocity: propeller 1

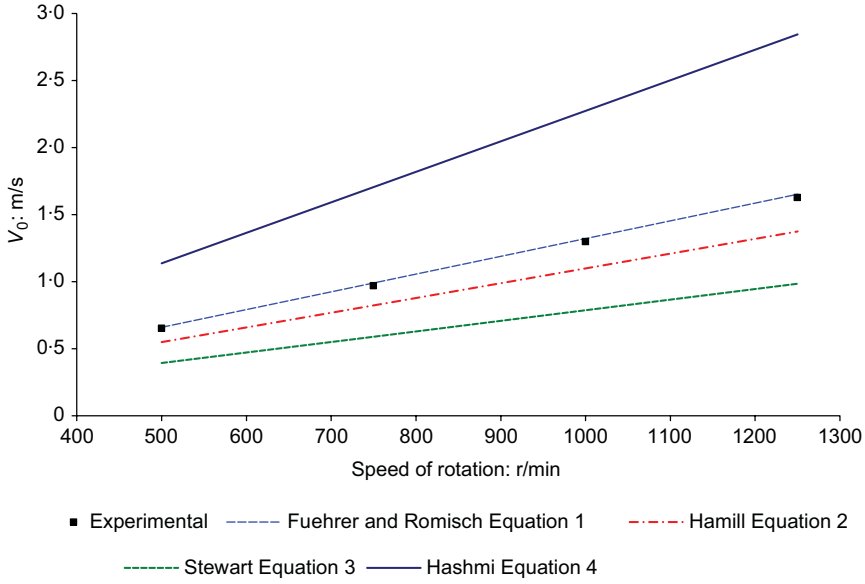

Figure 7. Comparison between measured and predicted axial efflux velocity: propeller 2

percentage difference of the same order of magnitude as that proposed by Prosser.

No existing equations are available to predict the magnitude of the maximum rotational velocity (U_0) along the efflux plane. A stepwise variable selection process was used to examine the influence of the independent variables in the study. The results of this analysis indicated that the variables that were most likely to influence the maximum rotational velocity, were the propeller speed of rotation (n), propeller diameter (D_p) and thrust coefficient (C_t), the same set of variables that control the magnitude of the axial component.

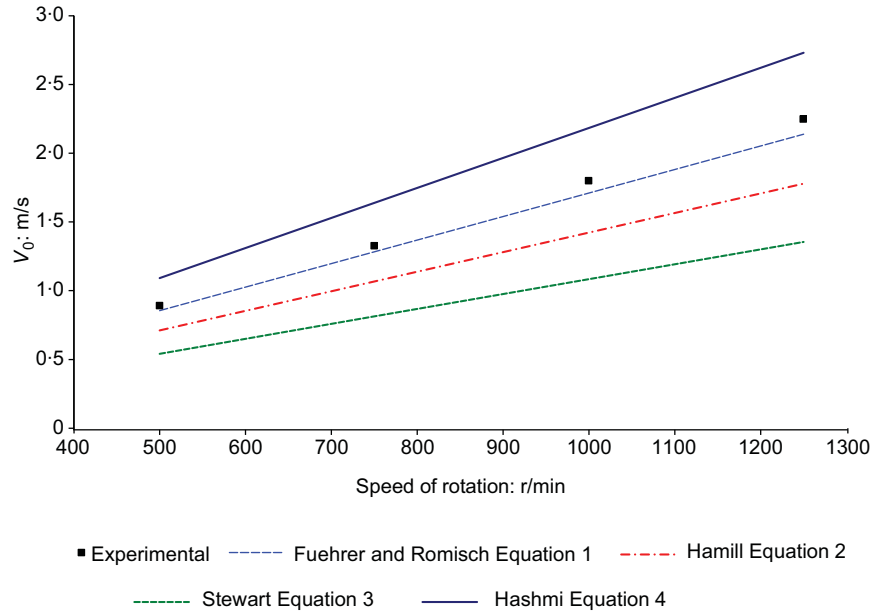

Figure 8. Comparison between measured and predicted axial efflux velocity: propeller 3

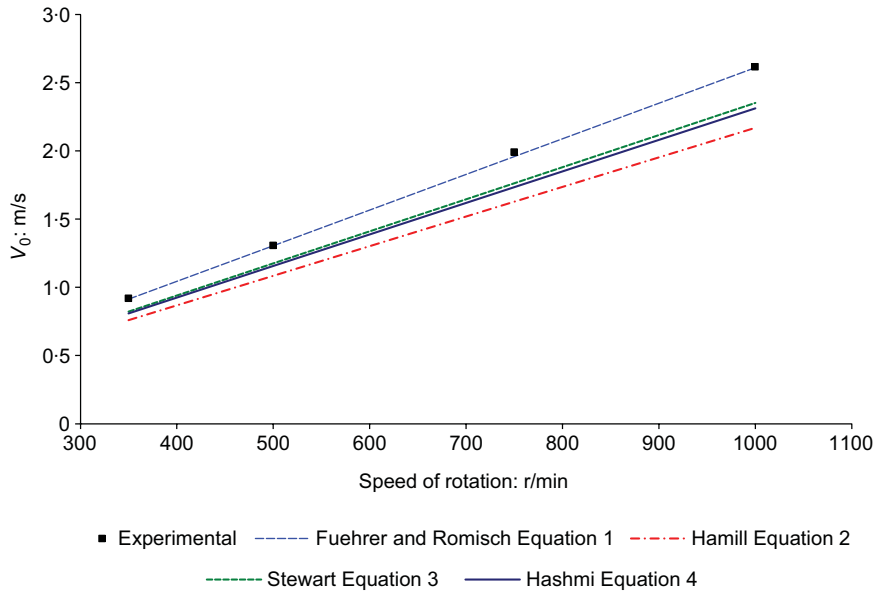

Figure 9. Comparison between measured and predicted axial efflux velocity: propeller 4

The correlation of these three independent variables on the dependent variable, U_0, was $R^2 = 0{\cdot}982$; the overall stepwise analysis can be found in Table 5, and Equation 10 is proposed as the most suitable equation for calculating the rotational efflux velocity.

$$U_0 = 1{\cdot}23 n^{1{\cdot}05} D_p^{0{\cdot}798} C_t^{1{\cdot}186} \quad (10)$$

The output solution of Equation 10 was plotted and compared with the measured efflux velocities and can be found in Figure 11, providing good comparisons across the full range of tested propellers.

Both Petersson *et al.* (1996) and Brewster (1997) investigated rotational velocity distributions along the initial efflux plane. The rotational velocity profile was shown to have two peak velocity values. One peak corresponded to the point at which the hub and the propeller blades were joined and the other was present at a point near to the tip of the propeller. Petersson *et al.* (1996) measured the first peak at $0{\cdot}15r/R_p$ and the second peak at $0{\cdot}65r/R_p$ from the propeller centreline. Brewster (1997) found the two peak velocities occurred at $0{\cdot}3r/R_p$ and $0{\cdot}8r/R_p$ from the propeller centreline.

Propeller radius $R_p = D_p/2$: mm	Experimental R_{m0}: mm (Average R_{m0} taken from left and right of propeller jet centreline)	Predicted R_{m0}: mm (Equation 5 proposed by Berger *et al.* (1981))
38	22·5	20·46
46	30	24·01
51·5	35	27·64
65·5	42·5	34·77

Table 4. Comparison of calculated and empirical measurements of the location of the maximum axial velocity along the efflux plane, R_{m0}

The measured locations of the peak velocities along the propeller hub/blade interface and near the propeller blade tip were found on average to give the position of the maximum rotational velocity at $r/R_p = 0{\cdot}12$, corresponding to the propeller hub/blade interface, and the second peak was located at approximately 75% from the propeller centreline: that is, $r/R_p = 0{\cdot}74$. This is in agreement with Petersson for the main peak location and between the proposed values of Petersson and Brewster for the second peak.

4.3 Radial efflux velocity

McGarvey (1996) found the magnitude of this component was approximately 30% of the axial velocity along the efflux plane.

Model	Variables entered	R^2	Error (SSE)
1	C_t	0·434	0·15069
2	n, C_t	0·866	0·07604
3	**n, D_p, C_t**	**0·982**	**0·02903**
4	n, D_p, C_t, BAR	0·98	0·0303
5	n, D_p, C_t, BAR, P'	0·98	0·032
6	n, D_p, C_t, BAR, P', N	0·859	0·171

Note: bold values indicate the selected output obtained from a stepwise regression analysis of all test variables.

Table 5. Stepwise model summary for rotational efflux velocity

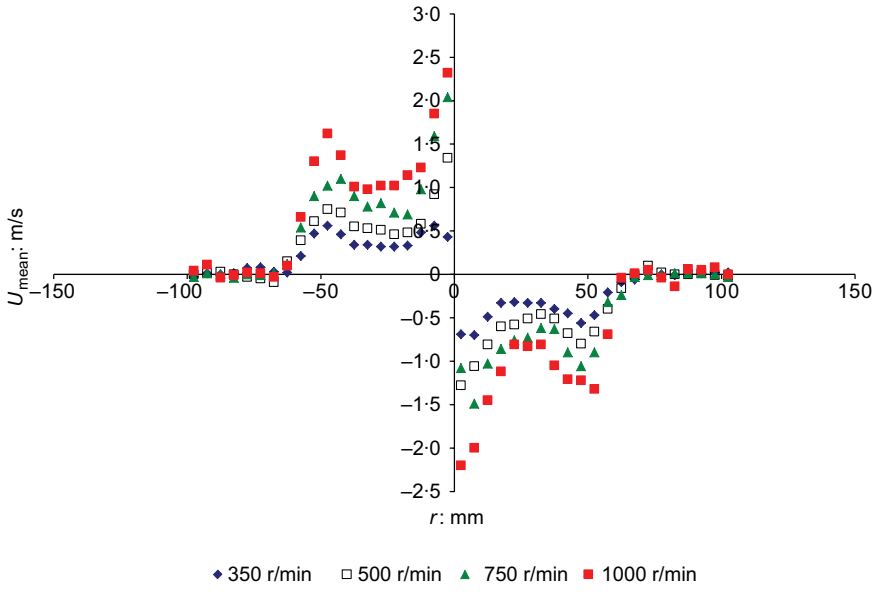

Figure 10. Rotational velocity distribution on efflux plane: propeller 4

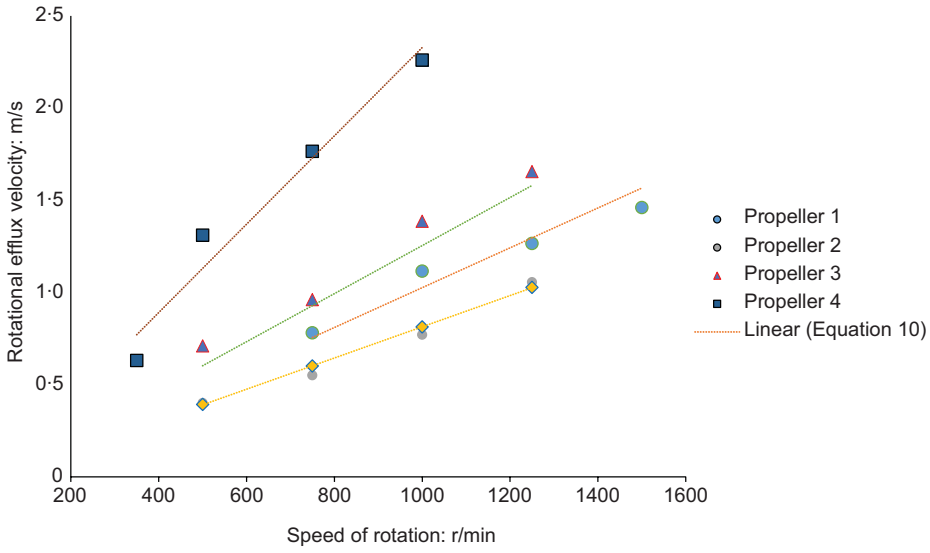

Figure 11. Comparison of measured rotational efflux velocity and Equation 10

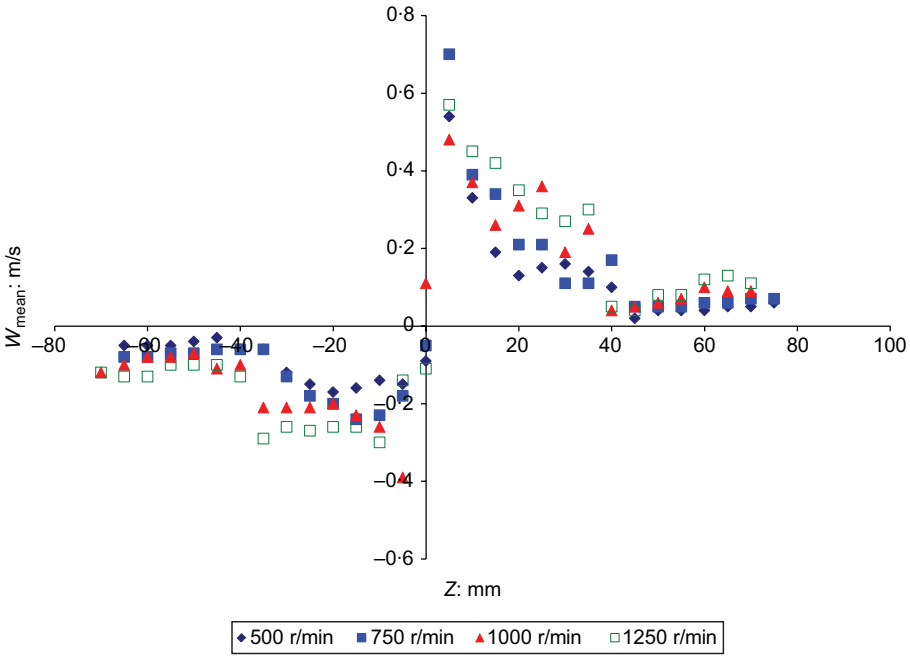

Figure 12. Radial velocity distributions on efflux plane: propeller 3

This magnitude of the radial velocity had a significant effect on the direction and diffusion of the jet flow within the initial stages of jet development. Table 3 shows the measured values of all the efflux velocities obtained in this investigation and it can be seen that the radial efflux velocity was consistently 20% of the maximum axial efflux value. Figure 12 shows the velocity distribution of the radial component of velocity, at all tested speeds, for propeller 3, and is again typical of the output obtained for each test propeller. As is the case of the rotational component the velocity direction can be seen to

change signs as it crosses through the propeller centre, with flow always occurring away from the centrepoint.

Examination of the literature showed no existing equations were available to determine the magnitude of the radial efflux velocity, W_0. In a manner similar to that employed for the previous components, Equation 11 was developed to allow a calculation to take place, and for which the coefficient of determination was 0·964.

$$11. \quad W_0 = 0{\cdot}153 n^{0{\cdot}986} D_p^{0{\cdot}719} C_t^{0{\cdot}344}$$

4.4 Resultant velocity

Figure 13 shows the resultant velocity profiles across the efflux plane for test propeller 2, and these are typical of the results obtained for all propellers. The shape of the distribution follows a trend similar to that of the axial efflux velocity across the propeller blade, with values beyond the hub increasing to a maximum, typical at $0{\cdot}6R_p$, and then decreasing rapidly to the jet edge. The large resultant component at the hub is due to the large rotational component found at that location. Outside that zone the direction of the resultant velocity is determined by the dominance of the axial and rotational velocities, and a 3D vector plot of the resultant velocity, Figure 14, shows output that clearly shows the swirling nature of the jet, a significant departure from the typical momentum jet. The magnitude of the efflux resultant is, in the cases of propellers 1, 2 and 4, approximately 7–9% larger than the axial value (propeller 3 was typically 2–4% larger than its efflux). The measured values appear on Table 3 alongside the component efflux values. Analysis of the resultant velocity and its dependence on the test variables reveals an expression similar in form to those derived for the other components, Equation 12. This equation has a standard error of 0·0112 and an R^2 value of 0·997.

$$12. \quad R_0 = 1{\cdot}2n0{\cdot}994 D_p^{0{\cdot}741} C_t^{0{\cdot}711}$$

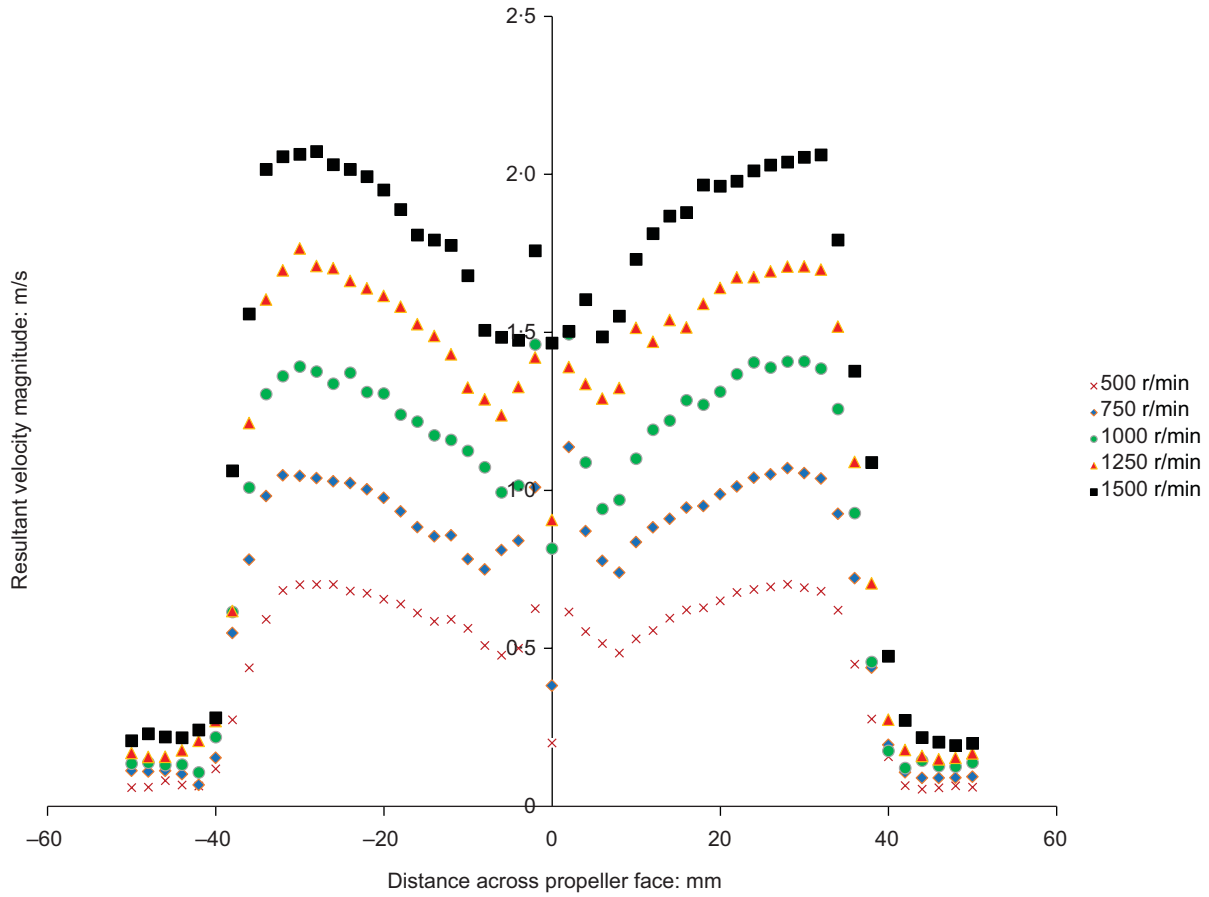

Figure 13. Distribution of the magnitude of the resultant velocity for propeller 2

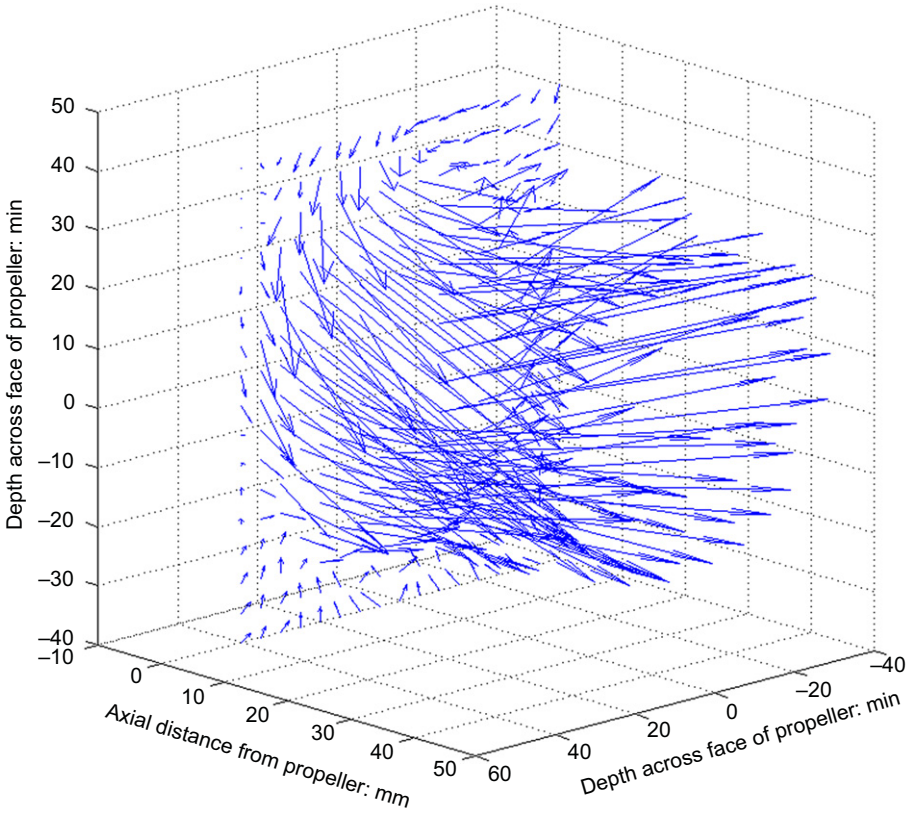

Figure 14. 3D resultant velocity distribution across efflux plane for propeller 2

5. Conclusion

The 3D nature of the efflux velocity was investigated for four propellers, whose characteristics ranged across typical operational values, using a 3D LDA measurement system over a very fine grid. The propellers were operated over a range of speeds of rotations typical of standard ship operating speeds.

The magnitude of a predicted axial efflux velocity was found to be dependent on the speed of rotation, propeller size and operating thrust coefficient. Comparison of measurements to current prediction methods found that while current methods predicted velocities well in some circumstances, as those equations were developed from limited test ranges, errors were present. A more general expression was derived, based on the extended test programme in this study, and it is recommended that it should be used in future calculations by design engineers.

The efflux rotational velocity was found to have two peak values on either side of the axis of rotation. Agreement with previous researchers was found with regards to the peak value at the hub edge; however, the peak value across the blade profile was found to occur at 75% of the propeller radius. The magnitude of this value was found to be some 70% of the axial value, 40% higher than previously thought, and for the first time an equation has been proposed that will allow the magnitude to be determined. The radial component, the smallest of all three components and some 20% of the axial value, was investigated and, as for the other major components, a method of prediction proposed.

The paper presents, for the first time, a discussion of the resultant velocity at efflux. The propeller jet on the efflux plane has measurable swirl, and the magnitude of the resultant component was found to be typically 8% higher than the standard calculated axial value. Calculations of the resultant efflux velocity should be made using the equation developed in the paper.

REFERENCES

Berger W, Felkel K, Hager M, Oebius H and Schale E (1981) Courant provoquè par les bateaux. Protection des berges et solution pour èviter l'èrosion du lit Haut Rhin. *Proceedings of the 25th Congress on Permanent*

International Association of Navigation Congresses (PIANC), Edinburgh, UK, Section I-1, pp. 51–69 (in French).

Bergh H and Cederwall K (1981) *Propeller Erosion in Harbours*. Hydraulics Laboratory, Royal Institute of Technology, Stockholm, Sweden, bulletin no. TRITA-VBI-107, pp. 139–143.

Blaauw HG and van de Kaa EJ (1978) *Erosion of Bottom and Sloping Banks Caused by the Screw Race of Manoeuvring Ships*. Delft Hydraulics Laboratory, Delft, the Netherlands, publication no. 202, pp. 1–12.

Brewster P (1997) *Modelling the Wash from a Ship's Propeller*. PhD thesis, Queen's University of Belfast, Northern Ireland.

Froehlich DC and Shea CC (2000) Screwed-up riprap: Sizing rock linings to resist ship propeller-jets. *Proceedings of Joint Conference on Water Resource Engineering and Water Resources Planning and Management 2000, Minnesota, USA*.

Fuehrer M and Römisch K (1977) *Effects of Modern Ship Traffic on Inland and Ocean Waterways and their Structures*. Permanent International Association of Navigation Congresses (PIANC), Brussels, Belgium, bulletin no. 24, section I-3, pp. 79–94.

Hamill GA (1987) *Characteristics of the Screw Wash of a Manoeuvring Ship and the Resulting Bed Scour*. PhD thesis, Queen's University of Belfast, Northern Ireland.

Hamill GA and Johnston HT (1993) The decay of maximum velocity within the initial stages of a propeller wash. *Journal of Hydraulic Research, International Association of Hydraulic Engineering and Research (IAHR)* **31(5)**: 605–613.

Hamill GA, Ryan D and Hughes DAB (2003) The formation of the jet produced by a rotating ship's propeller', *Proceedings of the Coasts & Ports Australasian Conference*, paper no. 249, pp. 1–8.

Hamill GA, McGarvey JA and Hughes DAB (2004) Determination of the efflux velocity from a ship's propeller. *Proceedings of the Institute of Civil Engineers – Maritime Engineering* **157(2)**: 83–91, http://dx.doi.org/10.1680/maen.2004.157.2.83.

Hashmi HN (1993) *Erosion of a Granular Bed at a Quay Wall by a Ship's Screw Wash*. PhD thesis, Queen's University of Belfast, Northern Ireland.

Lam W, Hamill GA, Robinson DJ and Raghunathan S (2012a) Semi-empirical methods for determining the efflux velocity from a ship's propeller. *Applied Ocean Research* **35(2012)**: 14–24.

Lam W, Robinson DJ, Hamill GA and Johnston HT (2012b) An effective method for comparing the turbulence intensity from LDA measurements and CFD predictions within a ship propeller jet. *Ocean Engineering* **52(2012)**: 105–124.

McGarvey JA (1996) *The Influence of the Rudder on the Hydrodynamics and the Resulting Bed Scour of a Ship's Screw Wash*. PhD thesis, Queen's University of Belfast, Northern Ireland.

Petersson P, Larson M and Jönsson L (1996) Measurements of the velocity field downstream of an impeller. *Journal of Fluids Engineering, Transactions of the American Society of Mechanical Engineers (ASME)* **118**: 602–610.

Prosser MJ (1986) *Propeller Induced Scour*. British Ports Association, London, UK, BHRA Report no. 2570, pp. l–33.

Qurrain RMM (1994) *Influence of the sea bed geometry and berth geometry on the hydrodynamics of the wash from a ship's propeller*. PhD thesis, Queen's University of Belfast, Northern Ireland.

Stewart DPJ (1992) *Characteristics of a Ship's Screw Wash and the Influence of Quay Wall Proximity*. PhD thesis, Queen's University of Belfast, Northern Ireland.

Sumer BM and Fredsoe J (2002) The mechanics of scour in the marine environment. *Advanced Series in Ocean Engineering, World Scientific* **17(x)**: 423–441.

Verhey HJ (1983) *The Stability of Bottom and Banks Subjected to Velocities in the Propeller Jet Behind Ships*. Delft Hydraulics Laboratory, Delft, the Netherlands, publication no. 303, pp. 1–11.

Verhey HJ, Blokland T, Bogaerts MP, Volger D and Weyde RW (1987) *Experiences in the Netherlands with quay structures subjected to velocities created by bow thrusters and main propellers of mooring and unmooring ships*. Permanent International Association of Navigation Congresses (PIANC), Brussels, Belgium, bulletin no. 58, pp. 69–88.

Yeh Y and Cummins HZ (1964) Localized fluid flow measurements with a He-Ne laser spectrometer. *Applied Physics Letters* **4**: 176–178.